Z. Angew. Math. Phys. (2024) 75:82

https://doi.org/10.1007/s00033-024-02224-9

Zeitschrift für angewandte Mathematik und Physik ZAMP

Sharp corner singularity of the White–Metzner model

Jonathan D. Evans and Christian A. Jones

Abstract. The stress singularity is determined using matched asymptotics for complete flow of a White–Metzner (WM) fluid around a re-entrant corner. The model is considered in the absence of a solvent viscosity, with power-law forms for the relaxation time and polymer viscosity. In this form, the model shares the same stress singularity as the upper convected Maxwell (UCM) model, but its wall boundary layers may be thinner or thicker than those for UCM depending upon the relative difference in the power-law exponents. If the exponent for the relaxation time is greater than that for the polymer viscosity, the boundary layer is narrower, whilst it is thicker if the polymer viscosity exponent exceeds that of the relaxation time. When the exponents are the same, the WM boundary layer thickness is the same size as that for UCM. A self-similar solution is derived for the stress and velocity fields and matched to both upstream and downstream boundary layers. Restrictions on the sizes of the power-law exponents are also given for validity of this solution.

Mathematics Subject Classification. 76A10, 35C06.

Keywords. Asymptotic results, Viscoelastic fluids, Corner flows, White–Metzner, Boundary layers, Stress singularity.

1. Introduction

We consider the steady planar flow of a White–Metzner fluid around a sharp corner. For this type of flow, the governing equations are given by

$$\nabla \cdot \mathbf{u} = 0, \tag{1}$$

$$\rho(\mathbf{u} \cdot \nabla)\mathbf{u} = -\nabla p + \nabla \cdot \boldsymbol{T}, \tag{2}$$

$$\boldsymbol{T} + \lambda(\dot{\gamma})\, \overset{\nabla}{\boldsymbol{T}} = 2\mu(\dot{\gamma})\boldsymbol{D}, \tag{3}$$

where $\mathbf{u}$ is the velocity field, p is the pressure and $\boldsymbol{T}$ is the extra-stress tensor. Equations (1) and (2) are conservation of mass and linear momentum, in which the viscoelastic liquid are taken as incompressible and the density ρ is assumed constant. Equation (3) is the constitutive equation of the White–Metzner fluid [1], where the upper convected derivative of extra-stress and rate-of-strain tensors are given by

$$\overset{\nabla}{\boldsymbol{T}} := (\mathbf{u} \cdot \nabla)\,\boldsymbol{T} - (\nabla \mathbf{u})\,\boldsymbol{T} - \boldsymbol{T}\,(\nabla \mathbf{u})^T, \qquad \boldsymbol{D} := \frac{1}{2}\left(\nabla \mathbf{u} + \nabla \mathbf{u}^T\right).$$

The relaxation time λ and viscosity μ are usually taken dependent on the second invariant of the rate-of-strain tensor through the shear rate

$$\dot{\gamma} := \sqrt{2D_{ij}D_{ij}}, \tag{4}$$

with summation convention implied.

The functional forms adopted for the relaxation time and viscosity are usually of Carreau type [2] (more generally Carreau-Yasuda). Parameters in these empirical relationships are determined by fitting the model to experimental data in steady shear flow [3]. Simpler power-law forms have also been adopted, particularly in earlier work [1]. These are particularly relevant here, since the shear rate is large due to

Published online: 10 April 2024

the stress singularity. As such, the Carreau type relationships are well-approximated by power-law forms, which we take as

$$\lambda(\dot{\gamma}) = \lambda_0 \dot{\gamma}^{q-1}, \quad \mu(\dot{\gamma}) = K_0 \dot{\gamma}^{n-1}, \tag{5}$$

where $q > 0, n > 0$ are flow behaviour indices with the additional positive constants λ_0 (units s^q) and K_0 (units $\mathrm{Pa} \cdot \mathrm{s}^n$). The upper convected Maxwell (UCM) model is obtained in the particular case $q = n = 1$, where the relaxation and viscosity are then both constant.

In use of the White–Metzner model, it is common to take both the flow behaviour indices to be the same, so that $q = n$. This is the case presented in [2], and referred to as the "Bird equality" by [4]. This assumption was also made in [3] when modelling both polyacrylamide (PAA) and polyethylene oxide (PEO) suspended in a solvent consisting of glycerol and water. For PAA, a range of n values between 0.30 and 0.73 inclusive were found; for the PEO solution, n was found to be between 0.48 and 1 (also inclusive). Further studies on polymer melts and solutions have found that q and n do not have to be equal. Examples include: a polyisobutylene and decalin solution [5] with flow behaviour indices of $n = 0.33$ and $q = 0.56$, and a polystyrene melt [6] with indices of $n = 0.17$ and $q = 0.064$.

As geometry for the problem, the above equations are taken to hold in the sector $0 < r < \infty,\ 0 \leq \theta \leq \pi/\alpha$, defined in polar coordinates centred at the corner apex. For sharp or re-entrant corners, we require the corner angle parameter $\alpha \in [1/2, 1)$. The flow direction is such that $\theta = 0$ is the upstream wall and $\theta = \pi/\alpha$ is the downstream wall.

The White–Metzner (WM) model [1] was originally introduced as a phenomenological generalisation to the upper convected Maxwell (UCM) model [2]. The advantages of the UCM model for modelling viscoelastic liquids are ability to capture fading memory, the relatively small number of adjustable parameters and its evolutionary stability. However, its disadvantages are that its predictions can be qualitatively different from experimental data, especially for concentrated solutions and polymer melts. The WM model keeps the same mathematical structure of the UCM differential constitutive equation, but aims to capture nonlinear viscoelastic behaviour by allowing the viscosity and relaxation time to depend upon the deformation rate. Its advantages lie in its flexibility to predict accurately viscometric behaviour (i.e. shear viscosity and first normal stress difference) of most polymeric fluids. Its disadvantages are that it fails to capture polymeric behaviour in more general flows [7], the model can lose evolutionary stability (in the Hadamard sense) due to the parameter dependency on the shear rate [8,9], and the equations still retain a stress singularity at finite elongational rates similar to the UCM model [9]. Despite these deficiencies, the WM model has still been used to model concentrated polymer solutions and melts in abrupt contractions [10,11] and cross-slot flows [3]. The parameter flexibility in the model allows it to model not just shear thinning behaviour of polymer melts [12], but also shear thickening behaviour of suspensions [13–15].

The motivation for studying the re-entrant corner problem for viscoelastic fluids is threefold:

1. Numerical schemes encounter convergence difficulties at sharp corners due to the presence of the stress singularity [16,17].
2. Asymptotics can be used to determine the limiting behaviour of the velocity and stress fields. This adds to the catalogue of known analytical behaviours for viscoelastic fluids (which is still relatively small compared to that for Newtonian fluids). The asymptotic behaviour can also be used to improve numerical schemes near the stress singularity.
3. The stress singularity is a test of the well-posedness of the viscoelastic model. It is not at all clear that a given viscoelastic model will have integrable stresses at such singular points.

Asymptotic results for the UCM model in this problem are discussed in [18–20]. As the radial distance to the corner vanishes, a three region structure is obtained. This comprises an outer region in which the upper convected derivative of stress dominates in the constitutive equation and then boundary layers symmetrically placed at the upstream and downstream walls. The boundary layers arise due to the viscometric stress behaviour that must be obtained at the walls from the no-slip condition. In the outer

region away from the walls, the stress and velocity behave as

$$\mathbf{T} = O(r^{-2(1-\alpha)}), \qquad \mathbf{v} = O(r^{\alpha(3-\alpha)-1}) \qquad \text{as } r \to 0. \tag{6}$$

The boundary layers are cusp like with their widths found to be

$$\delta = O(x^{2-\alpha}) \qquad \text{as } x \to 0, \tag{7}$$

where x is distance to the corner along either wall.

Initial steps at extending the above UCM results to the WM model were made in [4]. The approach followed identically that in [18], but is limited to the upstream and outer regions. The downstream region is omitted entirely and as such the problem remains incomplete. Here we rectify this deficiency, by solving the downstream boundary layer problem, which arguably is the most difficult part of the problem. The downstream solution is important, as it will show that the flow remains attached at the downstream wall and complete flow around the corner can theoretically exist.

2. Preliminary mathematical results

2.1. Hyperbolicity of the stress tensor

The evolutionary stability of the system of equations is a necessary physical requirement for all viscoelastic models. Conditions for the White–Metzner model to maintain its evolutionary character have been obtained by [8] and [9]. One of these is the positive definiteness of the conformation tensor

$$\boldsymbol{A} = \boldsymbol{T} + \frac{\mu}{\lambda}\boldsymbol{I}, \tag{8}$$

in terms of which the constitutive Eq. (3) is

$$\boldsymbol{A} + \lambda \overset{\nabla}{\boldsymbol{A}} = \lambda \left[\frac{D}{Dt}\left(\frac{\mu}{\lambda}\right) + \frac{\mu}{\lambda^2} \right] \boldsymbol{I}. \tag{9}$$

Following arguments similar to those in [21], we now derive an integral expression for the conformation tensor. Spatial Eulerian coordinates $\{\mathbf{x}\}$ may be related to the material Lagrangian coordinates $\{\mathbf{X}\}$ through the deformation gradient (and its associated inverse)

$$\boldsymbol{F} = \frac{\partial \mathbf{x}}{\partial \mathbf{X}}, \quad \boldsymbol{g} = \boldsymbol{F}^{-1},$$

with $F_{ij} = \frac{\partial x_i}{\partial X_j}$. It follows that

$$\nabla \mathbf{u} = \frac{D\boldsymbol{F}}{Dt}\boldsymbol{g}.$$

Furthermore, differentiating the equation $\boldsymbol{F}\boldsymbol{g} = \boldsymbol{I}$, we find that

$$\frac{D\boldsymbol{g}}{Dt} = -\boldsymbol{g}\nabla\boldsymbol{u}.$$

These two results allow us to conclude that

$$\boldsymbol{g}\, \overset{\nabla}{\boldsymbol{T}}\, \boldsymbol{g}^T = \frac{D}{Dt}\left(\boldsymbol{g}\boldsymbol{T}\boldsymbol{g}^T\right).$$

Consequently, the White–Metzner stress relation (3) may be written as

$$\frac{D}{Dt}\left(\boldsymbol{g}\boldsymbol{T}\boldsymbol{g}^T\right) + \frac{1}{\lambda}\boldsymbol{g}\boldsymbol{T}\boldsymbol{g}^T = -\frac{\mu}{\lambda}\frac{D}{Dt}\left(\boldsymbol{g}\boldsymbol{g}^T\right),$$

or equivalently as

$$\frac{D}{Dt}\left[\boldsymbol{g}\left(\boldsymbol{T} + \frac{\mu}{\lambda}\boldsymbol{I}\right)\boldsymbol{g}^T\right] + \frac{1}{\lambda}\boldsymbol{g}\left(\boldsymbol{T} + \frac{\mu}{\lambda}\boldsymbol{I}\right)\boldsymbol{g}^T = \left[\frac{D}{Dt}\left(\frac{\mu}{\lambda}\right) + \frac{\mu}{\lambda^2}\right]\boldsymbol{g}\boldsymbol{g}^T.$$

Integrating then gives

$$\boldsymbol{g}\left(\boldsymbol{T}+\frac{\mu}{\lambda}\boldsymbol{I}\right)\boldsymbol{g}^T=\int_{s=-\infty}^{t}\left[\frac{D}{Dt}\left(\frac{\mu}{\lambda}\right)+\frac{\mu}{\lambda^2}\right]\mathrm{e}^{\int\frac{1}{\lambda}\,ds'}\boldsymbol{g}\boldsymbol{g}^T\,ds\cdot\mathrm{e}^{-\int\frac{1}{\lambda}\,dt}.$$

Since $\boldsymbol{g}\boldsymbol{g}^T$ is positive definite, the positive definiteness of the left-hand-side of the above expression and hence the conformation tensor requires us to analyse the sign of

$$\frac{D}{Dt}\left(\frac{\mu}{\lambda}\right)+\frac{\mu}{\lambda^2}=\frac{K_0\dot\gamma^{n-2q-1}}{\lambda_0^2}\left[1+\lambda_0(n-q)\dot\gamma^{q-2}\frac{D\dot\gamma}{Dt}\right],$$

for nonzero shear rates. The only definitive parameter case, where positive definiteness is assured, is when $n=q$. The case $n\neq q$ depends upon the behaviour of the material derivative of the shear rate and no strong conclusions can be made.

2.2. Non-dimensionalisation

To non-dimensionalise the equations, we scale as follows:

$$\mathbf{x}=L\bar{\mathbf{x}},\quad \mathbf{u}=U\bar{\mathbf{u}},\quad p=\frac{K_0U^n}{L^n}\bar p,\quad \boldsymbol{T}=\frac{K_0U^n}{L^n}\bar{\boldsymbol{T}},$$

using representative length and velocity scales. The Reynolds and Weissenberg numbers are

$$\mathrm{Re}=\frac{\rho L^n}{U^{n-2}K_0}=\frac{\rho LU}{\left(\frac{K_0U^{n-1}}{L^{n-1}}\right)}\qquad\text{and}\qquad \mathrm{Wi}=\frac{\lambda_0U^q}{L^q}.$$

Noting that the re-entrant corner problem has no natural length or velocity scales, we may set these dimensionless constants to unity by choosing

$$U=L\lambda_0^{-1/q},\qquad L=\left(K_0\lambda_0^{\frac{2-n}{q}}\rho^{-1}\right)^{1/2}.$$

Inserting these scalings into the governing equations and dropping the bars on the variables, we obtain the resulting dimensionless equations:

$$\nabla\cdot\mathbf{u}=0, \tag{10}$$

$$(\mathbf{u}\cdot\nabla)\mathbf{u}=-\nabla p+\nabla\cdot\boldsymbol{T}, \tag{11}$$

$$\boldsymbol{T}+\dot\gamma^{q-1}\overset{\nabla}{\boldsymbol{T}}=2\dot\gamma^{n-1}\boldsymbol{D}. \tag{12}$$

2.3. Natural stress formulation

We first express Eqs. (10)–(12) in terms of the (dimensionless) conformation tensor $\boldsymbol{A}=\boldsymbol{T}+\dot\gamma^{n-q}\boldsymbol{I}$, leading to the equations

$$\nabla\cdot\mathbf{u}=0, \tag{13}$$

$$(\mathbf{u}\cdot\nabla)\mathbf{u}=-\nabla p-\nabla\left(\dot\gamma^{n-q}\right)+\nabla\cdot\boldsymbol{A}, \tag{14}$$

$$\boldsymbol{A}+\dot\gamma^{q-1}\overset{\nabla}{\boldsymbol{A}}=\left[\dot\gamma^{n-q}+\dot\gamma^{q-1}\left(\mathbf{u}\cdot\nabla\right)\left(\dot\gamma^{n-q}\right)\right]\boldsymbol{I}. \tag{15}$$

For analysis of the downstream wall and to give a complete solution around the corner, it is convenient to represent the conformation tensor with respect to a basis which is aligned with the flow [22,23]. This

is referred to as the natural stress basis, which consists of the velocity vector and an orthogonal vector given by

$$\mathbf{u} = (u, v)^T, \qquad \mathbf{w} = \left(-\frac{v}{u^2 + v^2}, \frac{u}{u^2 + v^2} \right)^T.$$

The conformation tensor may be expressed in terms of dyadic products of the vectors $\mathbf{u}$ and $\mathbf{w}$, in the form

$$\boldsymbol{A} = T_{uu}\mathbf{u}\mathbf{u}^T + T_{uw}(\mathbf{u}\mathbf{w}^T + \mathbf{w}\mathbf{u}^T) + T_{ww}\mathbf{w}\mathbf{w}^T, \tag{16}$$

where $T_{uu}(x, y), T_{uw}(x, y)$ and $T_{ww}(x, y)$ are variables aligned along streamlines, and the identity matrix $\boldsymbol{I}$ takes the form

$$\boldsymbol{I} = \frac{1}{\|\mathbf{u}\|^2}\mathbf{u}\mathbf{u}^T + \|\mathbf{u}\|^2\mathbf{w}\mathbf{w}^T.$$

The component form of (15) is

$$T_{uu} + \dot{\gamma}^{q-1}\,(\mathbf{u}\cdot\nabla)\,T_{uu} + 2\dot{\gamma}^{q-1}T_{uw}\,(\nabla\cdot\mathbf{w}) = \frac{\dot{\gamma}^{q-1}}{\|\mathbf{u}\|^2}\,(\mathbf{u}\cdot\nabla)\left(\dot{\gamma}^{n-q}\right) + \frac{\dot{\gamma}^{n-q}}{\|\mathbf{u}\|^2}, \tag{17}$$

$$T_{uw} + \dot{\gamma}^{q-1}\,(\mathbf{u}\cdot\nabla)\,T_{uw} + \dot{\gamma}^{q-1}T_{ww}\,(\nabla\cdot\mathbf{w}) = 0, \tag{18}$$

$$T_{ww} + \dot{\gamma}^{q-1}\,(\mathbf{u}\cdot\nabla)\,T_{ww} = \dot{\gamma}^{q-1}\|\mathbf{u}\|^2\,(\mathbf{u}\cdot\nabla)\left(\dot{\gamma}^{n-q}\right) + \|\mathbf{u}\|^2\dot{\gamma}^{n-q}, \tag{19}$$

where

$$\nabla\cdot\mathbf{w} = \frac{1}{\|\mathbf{u}\|^4}\left((u^2 - v^2)\left(\frac{\partial v}{\partial x} + \frac{\partial u}{\partial y}\right) + 4uv\frac{\partial u}{\partial x}\right).$$

Addressing the momentum Eq. (14),

$$\nabla\cdot\boldsymbol{A} = \mathbf{u}\cdot\nabla(T_{uu}\mathbf{u} + T_{uw}\mathbf{w}) + \mathbf{w}\cdot\nabla(T_{uw}\mathbf{u} + T_{ww}\mathbf{w}) + (T_{uw}\mathbf{u} + T_{ww}\mathbf{w})\nabla\cdot\mathbf{w},$$

so in component form we have

$$\begin{aligned}(\mathbf{u}\cdot\nabla)u = &-\frac{\partial p}{\partial x} - \frac{\partial}{\partial x}\left(\dot{\gamma}^{n-q}\right) + (\mathbf{u}\cdot\nabla)\left(T_{uu}u - \frac{T_{uw}v}{\|\mathbf{u}\|^2}\right) + (\mathbf{w}\cdot\nabla)\left(T_{uw}u - \frac{T_{ww}v}{\|\mathbf{u}\|^2}\right)\\ &+ \left(T_{uw}u - \frac{T_{ww}v}{\|\mathbf{u}\|^2}\right)\nabla\cdot\mathbf{w},\end{aligned} \tag{20}$$

$$\begin{aligned}(\mathbf{u}\cdot\nabla)v = &-\frac{\partial p}{\partial y} - \frac{\partial}{\partial y}\left(\dot{\gamma}^{n-q}\right) + (\mathbf{u}\cdot\nabla)\left(T_{uu}v + \frac{T_{uw}u}{\|\mathbf{u}\|^2}\right) + (\mathbf{w}\cdot\nabla)\left(T_{uw}v + \frac{T_{ww}u}{\|\mathbf{u}\|^2}\right)\\ &+ \left(T_{uw}v + \frac{T_{ww}u}{\|\mathbf{u}\|^2}\right)\nabla\cdot\mathbf{w}.\end{aligned} \tag{21}$$

2.4. Viscometric behaviour

An important part of the flow that our analysis needs to capture occurs near to the walls. In simple shear flow $u = \dot{\gamma}y$ with $\dot{\gamma} > 0$, (17)–(19) give the viscometric behaviour for the natural stresses as

$$T_{uu} = 2\frac{\dot{\gamma}^{n+q}}{u^2} + \frac{\dot{\gamma}^{n-q}}{u^2}, \qquad T_{uw} = \dot{\gamma}^n, \qquad T_{ww} = \dot{\gamma}^{n-q}u^2. \tag{22}$$

For large shear rates, we note $T_{uu} \sim 2\dot{\gamma}^{n+q}/u^2$, which will be the form relevant in the boundary layers.

3. Re-entrant corner problem

3.1. The outer or core flow solution

The outer region is taken to be close to the corner ($r \ll 1$), but away from the wall boundaries. The stress singularity ensures that the upper convected derivative of the stress dominates in the constitutive equation. The behaviour is very similar to the UCM case, which is well understood [18–20,23–26]. Consequently, introducing a streamfunction ψ, we quote the solution as

$$\begin{aligned}
&\psi \sim \frac{C_0}{\alpha^m} r^{m\alpha} \sin^m(\alpha\theta),\\
&\boldsymbol{T} \sim T_{uu}(\psi)\mathbf{u}\mathbf{u}^T + T_{uw}(\psi)\left(\mathbf{u}\mathbf{w}^T + \mathbf{w}\mathbf{u}^T\right) + T_{ww}(\psi)\mathbf{w}\mathbf{w}^T - \dot{\gamma}^{n-q}\boldsymbol{I},\\
&p \sim \frac{1}{2}T_{uu}(\psi)\|\mathbf{u}\|^2 \quad \text{as } r \to 0.
\end{aligned} \tag{23}$$

The streamfunction is a potential flow similarity solution, with amplitude C_0 set by the global flow and the index m is to be determined. The natural stress variables are constant along streamlines, and for self-similar behaviour, we take in power-law forms

$$T_{uu}(\psi) = d_1\left(\frac{\psi}{C_0}\right)^{m_1}, \quad T_{uw}(\psi) = d_2\left(\frac{\psi}{C_0}\right)^{m_2}, \quad T_{ww}(\psi) = d_3\left(\frac{\psi}{C_0}\right)^{m_3}, \tag{24}$$

where the d_i are arbitrary constants. The momentum equation links the indices m and m_1 through the relationship

$$m_1 = \frac{2}{m} - 2. \tag{25}$$

Matching this solution to the wall boundary layers determines the exponents as

$$\begin{aligned}
m &= \frac{2(n+q(3-2\alpha)+\alpha-1)}{2q+\alpha(n-q)}, \quad m_1 = \frac{2(1-\alpha)+q(3\alpha-4)+n(\alpha-2)}{\alpha-1+n+q(3-2\alpha)},\\
m_2 &= \frac{n(\alpha-1)}{\alpha-1+n+q(3-2\alpha)}, \quad m_3 = \frac{2(\alpha-1)+q(4-3\alpha)+n\alpha}{\alpha-1+n+q(3-2\alpha)}.
\end{aligned} \tag{26}$$

The exponents m and m_1 give the order of magnitude estimates in this region for the velocity, velocity gradient and extra-stress as

$$\mathbf{u} = O\left(r^{m\alpha-1}\right), \quad \nabla\mathbf{u} = O\left(r^{m\alpha-2}\right), \quad \boldsymbol{T} = O(r^{-2(1-\alpha)}). \tag{27}$$

In arriving at this solution, a priori assumptions are made in regards to the dominance of terms in the governing Eqs. (11) and (12). The leading order stress behaviour in (23) is a stretching solution, derived first for this problem in [24] and then more succinctly in [23]. The Cartesian stress analysis of [4] identified this solution as relevant to the WM model and stated four conditions for its validity. We summarise and modify them here as follows. The restriction $m > 1$ for subdominance of the inertia terms in the momentum equation is erroneous. A more restrictive condition is for the velocity field to remain finite and vanish at the corner, which from (27) requires $m\alpha > 1$. The dominance of the upper convected derivative over the relaxation and rate-of-strain terms in (12) gives further restrictions on m. Taken together, these give

$$\text{a) } 1 < \alpha m < 2 \quad \text{and} \quad \text{b) } \alpha m(q-n) < 2(1+\alpha+q-n), \tag{28}$$

to hold for all re-entrant corner angles $1/2 \le \alpha < 1$. The first inequality in a) gives

$$2\alpha(1-\alpha) < \alpha n + (7\alpha - 4\alpha^2 - 2)q, \tag{29}$$

this region being bounded by

$$1 = n + q, \tag{30}$$

whilst the second inequality in a) gives $-2q < \frac{\alpha}{1-\alpha}$, which is automatically satisfied for non-negative q. Finally, b) gives

$$n - q < \frac{1}{1-\alpha}. \tag{31}$$

In the parameter case $n = q$, (30) suggests an α independent lower bound of $n = 1/2$ whilst (31) is not restrictive. Consequently, we have $n = q \geq 1/2$, with no upper bound.

More generally, when $n \neq q$, it is convenient to discuss the shear thinning ($0 < n < 1$) and shear thickening ($n > 1$) cases separately. In the shear thinning case, (30) provides the α independent bound and thus $q > 1 - n$, since (31) is not restrictive in this case. For $1 \leq n \leq 2$, (30) and (31) are not restrictive, so $q > 0$. Finally, for $n > 2$, (30) is not restrictive but (31) suggests $q > n - 2$. A pictorial summary is given later in the discussion section.

To determine the scalings for the upstream or downstream layers, we require the limiting behaviour of the outer solution (23) as the walls are approached. Focusing on the upstream wall, we have that as $y \to 0^+$:

$$\begin{aligned}
&\psi \sim C_0 x^{m(\alpha-1)} y^m, \quad u \sim m C_0 x^{m(\alpha-1)} y^{m-1}, \quad v \sim -m(\alpha-1) C_0 x^{m(\alpha-1)-1} y^m, \\
&T_{uu} \sim d_1 \left(x^{(\alpha-1)} y \right)^{mm_1}, \quad T_{uw} \sim d_2 \left(x^{(\alpha-1)} y \right)^{mm_2}, \quad T_{ww} \sim d_3 \left(x^{(\alpha-1)} y \right)^{mm_3}, \\
&p \sim \frac{1}{2} m^2 C_0^2 d_1 x^{2(\alpha-1)}, \quad \dot{\gamma} \sim m(m-1)|C_0| x^{m(\alpha-1)} y^{m-2}.
\end{aligned} \tag{32}$$

Stress boundary layers at the walls are required, since the outer solution does not give viscometric behaviour appropriate to the WM model as recorded in Sect. 2.4. The stress relaxation and rate-of-strain terms need to be recovered in the WM constitutive equation, the analysis of which we address next.

3.2. The upstream boundary layer

To derive the leading order boundary layer equations, we need to systematically compare terms in the governing equations. This is best done through introducing an artificial small parameter, representing the length scale from the corner on which we expect the structure to exist. We thus set

$$x = \epsilon X, \tag{33}$$

where $0 < \epsilon \ll 1$, and consider the region $X = O(1)$. Since the parameter is introduced artificially, it scales from the equations and its actual size can only be determined from numerical solution of a complete flow problem that contains the re-entrant corner. In addition, we set

$$\begin{aligned}
&y = \delta Y, \ \psi = \theta \bar{\psi}, \ u = \frac{\theta}{\delta} \bar{u}, \ v = \frac{\theta}{\epsilon} \bar{v}, \ p = \epsilon^{2(\alpha-1)} \bar{p}, \\
&T_{uu} = \theta^{m_1} \bar{T}_{uu}, \ T_{uw} = \theta^{m_2} \bar{T}_{uw}, \ T_{ww} = \theta^{m_3} \bar{T}_{ww},
\end{aligned} \tag{34}$$

where the gauge $\delta(\epsilon)$ represents the boundary layer width to be determined and $\theta = \epsilon^{m(\alpha-1)} \delta^m$ is introduced for convenience. Under these scalings, at leading order in ϵ, the momentum equations become

$$0 = -\frac{\partial \bar{p}}{\partial X} + \left(\bar{\mathbf{u}} \cdot \bar{\nabla} \right) \left(\bar{T}_{uu} \bar{u} \right) + \frac{\partial \bar{T}_{uw}}{\partial Y}, \tag{35}$$

$$0 = \frac{\partial \bar{p}}{\partial Y}, \tag{36}$$

and the WM constitutive equations give

$$\bar{T}_{uu} + \left| \frac{\partial \bar{u}}{\partial Y} \right|^{q-1} \left(\bar{\mathbf{u}} \cdot \bar{\nabla} \right) \bar{T}_{uu} + 2 \left| \frac{\partial \bar{u}}{\partial Y} \right|^{q-1} \bar{T}_{uw} \frac{\partial}{\partial Y} \left(\frac{1}{\bar{u}} \right) = 0. \tag{37}$$

$$\bar{T}_{uw} + \left| \frac{\partial \bar{u}}{\partial Y} \right|^{q-1} \left(\bar{\mathbf{u}} \cdot \bar{\nabla} \right) \bar{T}_{uw} + \left| \frac{\partial \bar{u}}{\partial Y} \right|^{q-1} \bar{T}_{ww} \frac{\partial}{\partial Y} \left(\frac{1}{\bar{u}} \right) = 0, \tag{38}$$

$$\bar{T}_{ww} + \left|\frac{\partial \bar{u}}{\partial Y}\right|^{q-1} \left(\bar{\mathbf{u}} \cdot \bar{\nabla}\right) \bar{T}_{ww} = \bar{u}^2 \left(\left|\frac{\partial \bar{u}}{\partial Y}\right|^{q-1} \left(\bar{\mathbf{u}} \cdot \bar{\nabla}\right) \left|\frac{\partial \bar{u}}{\partial Y}\right|^{n-q} + \left|\frac{\partial \bar{u}}{\partial Y}\right|^{n-q} \right). \tag{39}$$

The dominant balance required to obtain these equations requires

$$\delta = \epsilon^{\frac{1+(1-\alpha)mq}{1+(m-2)q}} = \epsilon^{\frac{n+(3-2\alpha)q}{n+q}}, \tag{40}$$

with the m and the m_1, m_2, m_3 as stated in (26). The system of PDEs (35)–(39) is completed with the no-slip conditions

$$\text{on } Y = 0: \qquad \bar{\psi} = \frac{\partial \bar{\psi}}{\partial Y} = 0, \tag{41}$$

and the outer solution matching conditions

$$\begin{aligned} &\text{as } Y \to \infty: \qquad \bar{\psi} \sim C_0 X^{m(\alpha-1)} Y^m, \quad \bar{p} \sim \frac{1}{2} m^2 C_0^2 d_1 X^{2(\alpha-1)}, \\ &\bar{T}_{uu} \sim d_1 \left(\frac{\bar{\psi}}{C_0}\right)^{m_1}, \quad \bar{T}_{uw} \sim d_2 \left(\frac{\bar{\psi}}{C_0}\right)^{m_2}, \quad \bar{T}_{ww} \sim d_3 \left(\frac{\bar{\psi}}{C_0}\right)^{m_3}. \end{aligned} \tag{42}$$

The pressure in this region is thus its limiting behaviour from the outer solution and may be written as

$$\bar{p} = p_0 X^{2(\alpha-1)}, \quad p_0 = \frac{1}{2} m^2 C_0^2 d_1. \tag{43}$$

3.2.1. Similarity solution. The system of Eqs. (35)–(39), together with the conditions (41) and (42) possess a similarity solution in the variable

$$\chi = X^{-a} Y, \tag{44}$$

with

$$\begin{aligned} &\bar{\psi} = X^b f(\chi), \quad \bar{p} = X^{2\alpha-2} p_0, \quad \bar{T}_{uu} = X^{bm_1} t_{uu}(\chi), \\ &\bar{T}_{uw} = X^{bm_2} t_{uw}(\chi), \quad \bar{T}_{ww} = X^{bm_3} t_{ww}(\chi). \end{aligned} \tag{45}$$

where, for convenience, we have introduced

$$a = \frac{n + (3-2\alpha)q}{n+q}, \qquad b = (\alpha - 1 + a)m = \frac{2(n + (3-2\alpha)q + \alpha - 1)}{n+q}. \tag{46}$$

The velocity components are

$$\bar{u} = X^{b-a} f'(\chi), \qquad \bar{v} = X^{b-1}(a\chi f' - bf),$$

and our system of PDEs reduces to the four ODEs:

$$0 = 2(1-\alpha)p_0 - bff' t'_{uu} + t'_{uw} + \left[(bm_1 + b - a)\left(f'\right)^2 - bff''\right] t_{uu}, \tag{47}$$

$$-bft'_{uu} + (bm_1 f' + |f''|^{1-q}) t_{uu} - 2\frac{f''}{(f')^2} t_{uw} = 0, \tag{48}$$

$$-bft'_{uw} + (bm_2 f' + |f''|^{1-q}) t_{uw} - \frac{f''}{(f')^2} t_{ww} = 0, \tag{49}$$

$$-bft'_{ww} + (bm_3 f' + |f''|^{1-q}) t_{ww} = (f')^2 |f''|^{n-q} \left[|f''|^{1-q} - (n-q)\left[(2a-b)f' + b\frac{ff''}{|f''|^2} f'''\right]\right], \tag{50}$$

with boundary conditions

$$\text{at } \chi = 0: \qquad f = f' = 0, \tag{51}$$

$$\text{as } \chi \to \infty: \qquad f \sim C_0 \chi^m, \quad t_{uu} \sim d_1 \chi^{mm_1}, t_{uw} \sim d_2 \chi^{mm_2}, \quad t_{ww} \sim d_3 \chi^{mm_3}. \tag{52}$$

3.2.2. Upstream numerical solution. Since $\chi = 0$ is a singular point for the equations (47)–(50), it will be convenient in their numerical solution to use the two-term asymptotic wall behaviours. As $\chi \to 0$, we have

$$f \sim \frac{1}{2} f_2 \chi^2 + \frac{1}{6} f_3 \chi^3, \tag{53}$$

$$\chi^2 t_{uu} \sim 2|f_2|^{n+q-2} + \frac{2|f_2|^{n+q-2}}{f_2} \left[f_3(n+q-1) - (2a(n-q) + b(m_1+m_2+m_3-n+q))|f_2|^{q+1} \right] \chi, \tag{54}$$

$$t_{uw} \sim f_2 |f_2|^{n-1} + \left[(2a - 3b - 2bm_1)|f_2|^{n+q} + 2(\alpha - 1)p_0 \right] \chi, \tag{55}$$

$$\chi^{-2} t_{ww} \sim |f_2|^{n+2-q} + f_2 |f_2|^{n-q} \left[f_3(1+n-q) + (2a(q-n) + b(1+n-q-m_3))|a|^{q+1} \right], \tag{56}$$

where $f_2 = f''(0)$ is nonzero, $f_3 = f'''(0)$ and

$$p_0 = \frac{\left[2a(q-n-1) + b(4 + 2m_1 - m_2 - m_3 + n - q) \right] |f_2|^{n+q} + n f_3 |f_2|^{n-1}}{2(\alpha - 1)}. \tag{57}$$

Eliminating t'_{uu} and t'_{uw} in (47) using (48) and (49) gives, for $q \neq 1$, a nonlinear equation for f'' in the form

$$L f'' + K |f''|^{1-q} + Q = 0, \tag{58}$$

where

$$L = bf t_{uu} - \frac{2 t_{uw}}{f'} + \frac{t_{ww}}{bf (f')^2}, \quad K = f' t_{uu} - \frac{t_{uw}}{bf}, \quad Q = 2p_0(\alpha - 1) - (b - a)(f')^2 t_{uu} - \frac{m_2 f' t_{uw}}{f}.$$

In the case $n = q$, Eq. (58) with (48)–(50) gives a fifth-order system for $(f, f', t_{uu}, t_{uw}, t_{ww})$. However, when $n \neq q$, a third-order derivative of f enters (50) and the overall system becomes sixth-order. Differentiating Eq. (58) gives that

$$f''' = -\frac{Q' + K' |f''|^{1-q} + L' f''}{L + (1-q) K |f''|^{-(1+q)}}. \tag{59}$$

The system of equations to solve is now (59) with (48)–(50) for $(f, f', f'', t_{uu}, t_{uw}, t_{ww})$.

In both $n = q$ and $n \neq q$ cases we solve the system of equations as an initial-value problem, imposing the asymptotic wall behaviour (53)–(56) at sufficiently small positive values of χ.

The system of equations (47)–(50) with (53)–(56) contain two free parameters (f_2, p_0), since f_3 is fixed through (57). In this upstream region, the flow is towards the corner apex and thus $f_2 < 0$, whilst the pressure gradient is negative so that $p_0 > 0$. Since our system of equations is invariant under the scaling

$$\chi = \Gamma \hat{\chi}, \; f = \Gamma^{\frac{2q-1}{q}} \hat{f}, \; p_0 = \Gamma^{-\frac{n+q}{q}} \hat{p_0}, \; t_{uu} = \Gamma^{\frac{2-3q-n}{q}} \hat{t}_{uu}, \; t_{uw} = \Gamma^{-\frac{n}{q}} \hat{t}_{uw}, \; t_{ww} = \Gamma^{\frac{3q-n-2}{q}} \hat{t}_{ww},$$

we can take $\Gamma = p_0^{-\frac{q}{n+q}}$ and so, without loss of generality, set $p_0 = 1$. The upstream problem is thus reduced to a single parameter family of solutions, parameterised by the wall shear rate constant f_2, which is set by the incoming external flow. Solving the IVP for fixed f_2 will determine the far-field constants (C_0, d_1, d_2, d_3), where $d_1 = 2/m^2 C_0^2$ from (43) with $p_0 = 1$. We remark that the scaling in p_0 formulates the problem in terms of similarity parameters

$$f_2 \Gamma^{\frac{1}{q}}, \quad C_0 \Gamma^{m + \frac{1-2q}{q}}, \quad d_1 \Gamma^{m m_1 + \frac{n+3q-2}{q}}, \quad d_2 \Gamma^{m m_2 + \frac{n}{q}}, \quad d_3 \Gamma^{m m_3 + \frac{n+2-3q}{q}},$$

which can be used to map the $p_0 = 1$ solution to more general p_0 values.

We now give the numerical solutions for the upstream layer, focusing on the case $n = q$. To distinguish from the downstream layer, we add a subscript u to the wall and far-field constants so that

$$(f_2, f_3, p_0, C_0, d_1, d_2, d_3) = (f_{2u}, f_{3u}, p_{0u}, C_{0u}, d_{1u}, d_{2u}, d_{3u}). \tag{60}$$

As just discussed, we take $p_{0u} = 1$ so that

$$f_{3u} = \frac{2n(\alpha-1) - (\alpha-1)(3n-2)|f_{2u}|^{2n}}{n^2|f_{2u}|^{n-1}}.$$

For numerical implementation, it is preferable to use the scaled natural stress variables suggested in (54)–(56), namely

$$\chi^2 t_{uu}, \quad t_{uw} \quad \text{and} \quad \chi^{-2} t_{ww}, \tag{61}$$

which remain finite and nonzero at the wall. With these new natural stress variables, we solve Eqs. (48)–(50) alongside Eq. (58) using MATLAB's ode15s solver. In particular, roots of (58) are found via the inbuilt fzero routine. Figure 1 plots the solution of the boundary layer equations for $(f, \chi^2 t_{uu}, t_{uw}, \chi^{-2} t_{ww})$ in the case $n = q$, where $n = 0.5, 1$ and 2. In all three cases, $f_{2u} = -1$, $p_{0u} = 1$, $\alpha = 2/3$ and $[\chi_0, \chi_\infty] = [10^{-6}, 10^6]$. Verification of the large χ asymptotic behaviour is observed in Fig. 2, where plots of the variables $(f, \chi^2 t_{uu}, t_{uw}, \chi^{-2} t_{ww})$ scaled by their far-field conditions are presented.

Figure 3 shows the variation of C_{0u} with f_{2u} when $p_{0u} = 1$ and for selected $n = q$ values. As observed by [25] for Oldroyd-B, it illustrates that there is a lower value to the streamfunction coefficient at which the wall shear stress will vanish. At this point, separation will occur at the upstream wall with reverse flow near the boundary and an upstream dividing streamline emanating from the corner. Compared to the UCM case $n = q = 1$, this minimum C_{0u} value is greater (less negative) for shear thickening $n = q > 1$ and smaller (more negative) for shear thinning $n = q < 1$.

3.3. The downstream boundary layer

Remaining in the case $n = q$, we now turn our attention to the downstream part of the problem. Firstly, we note that via the transformation

$$\psi \to -\psi, \quad y \to -y, \quad \text{and} \quad t_{uw} \to -t_{uw}, \tag{62}$$

we can consider the downstream layer relative to the Cartesian axes of the upstream layer, so that the same governing equations hold. Physically, this corresponds to a re-orientation of the axes and reversal of the flow direction. Therefore, we may solve Eqs. (47)–(50) for the downstream layer. For clarity, we attach a label d to the downstream wall and far-field constants, so that

$$(f_2, f_3, p_0, C_0, d_1, d_2, d_3) = (f_{2d}, f_{3d}, p_{0d}, C_{0d}, d_{1d}, d_{2d}, d_{3d}), \tag{63}$$

where

$$f_{3d} = \frac{2n(\alpha-1)p_{0d} - (\alpha-1)(3n-2)|f_{2d}|^{2n}}{n^2|f_{2d}|^{n-1}}.$$

Since the downstream layer can be viewed relative to the upstream layer by our transformation (62), we also know that the downstream pressure and far-field constants can be related to those of the upstream via

$$p_{0d} = p_{0u}, \quad C_{0d} = -C_{0u}, \quad d_{1d} = d_{1u}, \quad d_{2d} = -d_{2u}, \quad d_{3d} = d_{3u}. \tag{64}$$

Again, this means that without loss of generality, we may consider the case $p_{0u} = 1$. To solve the similarity equations in the downstream layer, we set up a boundary value problem on a truncated domain $[\chi_0, \chi_\infty]$ using Eqs. (48)–(50) and (58), imposing the far-field behaviours (52) at χ_∞ and the wall behaviours (53)–(56) at χ_0. Following the BVP formulation discussed in [19], we specify the values of the constants (C_{0d}, d_{2d}, d_{3d}), leaving the wall parameter f_{2d} to be determined.

The solution to the downstream problem is computed using MATLAB's `bvp4c` finite difference solver, with scaled stress variables introduced in Eq. (61), and implemented boundary conditions

$$\text{at } \chi = \chi_0: \quad t_{uw} = 2^n f|f|^{n-1}\chi_0^{-2n}, \quad \chi_0^{-2} t_{ww} = 4f^2\chi_0^{-4} \tag{65}$$

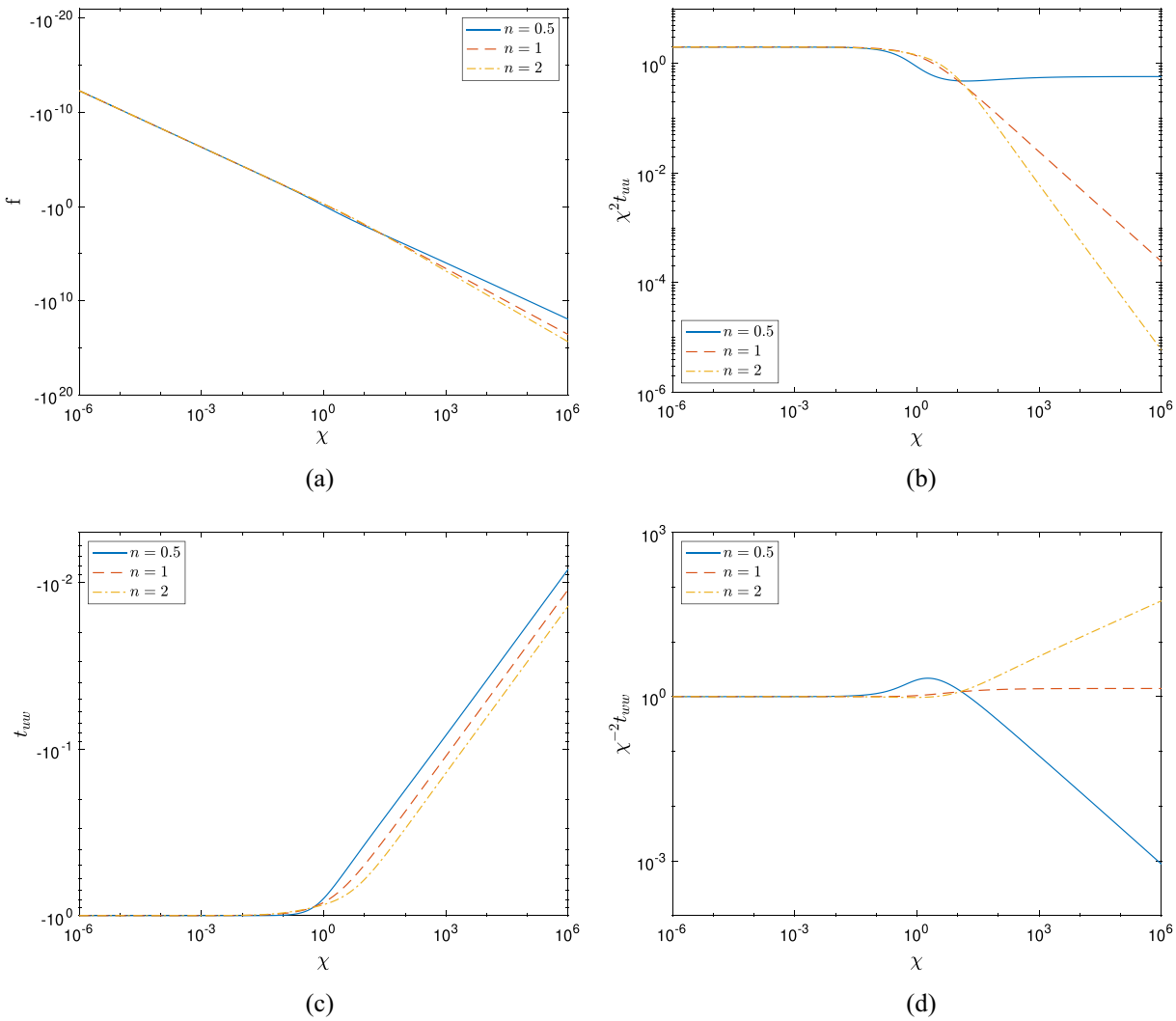

FIG. 1. The solution profiles found from solving the upstream problem for $n = 0.5$, (solid line), $n = 1$ (dashed line) and $n = 2$ (dot-dashed line). Figure **a** shows the streamfunction f. Figures **b**–**d** show the scaled stress variables $\chi^2 t_{uu}$, t_{uw} and $\chi^{-2} t_{ww}$, respectively. In each case, $f_{2u} = -1$, $p_{0u} = 1$, $\alpha = 2/3$ and the solution interval is $[\chi_0, \chi_\infty] = [10^{-6}, 10^6]$

$$\text{at } \chi = \chi_\infty : \quad f = C_{0d}\chi_\infty^{\frac{2(2-\alpha)n+\alpha-1}{n}}, \quad t_{uw} = d_{2d}\chi_\infty^{\alpha-1}, \quad \chi_\infty^{-2} t_{ww} = d_{3d}\chi_\infty^{\frac{2(1-\alpha)(n-1)}{n}}. \tag{66}$$

In using `bvp4c`, we set the relative and absolute error tolerances to be `RelTol` $= 10^{-3}$ and `AbsTol` $= 10^{-6}$, respectively, and supply an initial guess of the form

$$f = \begin{cases} \frac{1}{2} f_{2d}\chi^2 + \left(C_{0d} - \frac{1}{2} f_{2d}\right)\chi^3, & \chi \le 1, \\ C_{0d}\chi^{\frac{2(2-\alpha)n+\alpha-1}{n}}, & \chi > 1, \end{cases}$$

$$f' = \begin{cases} f_{2d}\chi + \left(C_{0d}\left(\frac{2(2-\alpha)n+\alpha-1}{n}\right) - f_{2d}\right)\chi^2, & \chi \le 1, \\ C_{0d}\frac{2(2-\alpha)n+\alpha-1}{n}\chi^{\frac{2(2-\alpha)n+\alpha-1}{n}-1}, & \chi > 1, \end{cases}$$

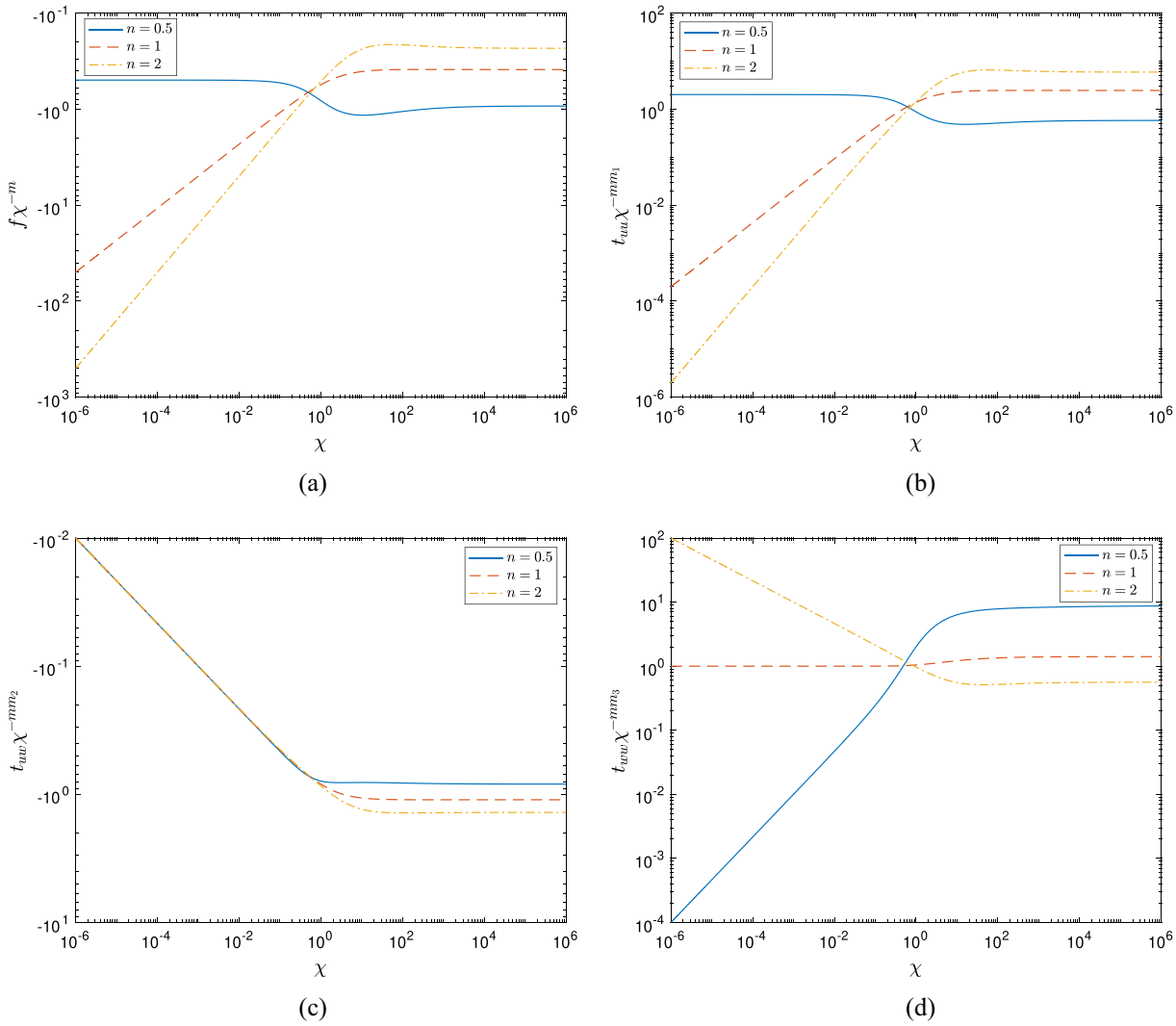

FIG. 2. The solution profiles found from solving the upstream problem for $n = 0.5$, (solid line), $n = 1$ (dashed line) and $n = 2$ (dot-dashed line), scaled by their expected far-field behaviour. Figure **a** shows the streamfunction f. Figures **b–d** show the scaled stress variables $\chi^2 t_{uu}$, t_{uw} and $\chi^{-2} t_{ww}$, respectively. In each case, $f_{2u} = -1$, $p_{0u} = 1$, $\alpha = 2/3$ and the solution interval is $[\chi_0, \chi_\infty] = [10^{-6}, 10^6]$

$$\chi^2 t_{uu} = \begin{cases} 2|f_{2d}|^{2n-2} + \left(d_{1d} - 2|f_{2d}|^{2n-2}\right)\chi, & \chi \le 1, \\ d_{1d}\chi^{\frac{2[(2\alpha-3)n+1-\alpha]}{n}+2}, & \chi > 1, \end{cases}$$

$$t_{uw} = \begin{cases} f_{2d}|f_{2d}|^{n-1} + \left(d_{2d} - f_{2d}|f_{2d}|^{n-1}\right)\chi, & \chi \le 1, \\ d_{2d}\chi^{\alpha-1}, & \chi > 1, \end{cases}$$

$$\chi^{-2} t_{ww} = \begin{cases} f_{2d}^2 + (d_{3d} - f_{2d}^2)\chi, & \chi \le 1, \\ d_{3d}\chi^{\frac{2(\alpha-1)(n-1)}{n}}, & \chi > 1. \end{cases}$$

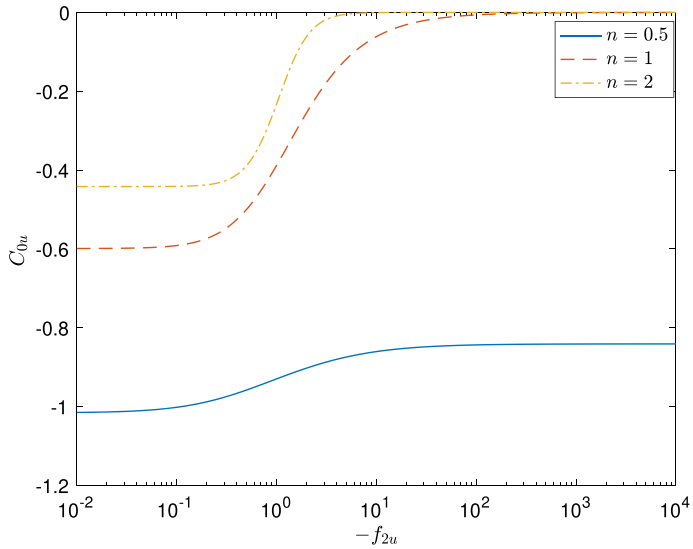

FIG. 3. The variation of C_{0u} with $-f_{2u}$ for $n = 0.5$, (solid line), $n = 1$ (dashed line) and $n = 2$ (dot-dashed line) when $p_{0u} = 1$. In all cases, we consider $\alpha = 2/3$

This initial guess is based on the leading order asymptotic behaviours for small and large χ with enforced continuity at $\chi = 1$, and is posed on a smaller domain contained within the interval $[\chi_0, \chi_\infty] = [10^{-3}, 10^4]$ with 1000 equally spaced mesh points. Specifying the exact starting domain is dependent on the value of the power-law exponent n, with the domain decreasing in size as we deviate from the UCM case ($n = 1$). The solution is then continued onto the full interval via usage of MATLAB's `bvpinit` procedure. We also require an estimate of the parameter f_{2d} to use our initial guess; this is again dependent on the value of n. For $n = 1$, the estimate was taken as $f_{2d} = 1$, increasing as the value of n decreased (and vice versa). Plots of the downstream variables for $n = 0.5$, $n = 1$ and $n = 1.4$ are shown in Figs. 4, 5 and 6, together with plots of four functions which can be used to estimate the downstream wall parameter f_{2d} in the case where $f_{2u} = -1, p_{0u} = 1$ and $\alpha = 2/3$. In each case, the required values of (C_{0d}, d_{2d}, d_{3d}) were set via the solution of the upstream layer on the interval $[10^{-6}, 10^6]$.

4. Discussion

The White–Metzner model is a phenomenological generalisation of the UCM model, where the relaxation time and polymer viscosity are functions of the second invariant of the rate-of-strain tensor. The model is nonlinear (rather than quasilinear like UCM) and allows for more realistic behaviour exhibited by molten polymers than the simple behaviours given by the UCM model.

A self-similar solution (23) has been constructed for the model for any re-entrant corner angle and matched to both upstream and downstream wall boundary layers. Compared to the UCM model, the order of magnitude estimates (27) show that the stress singularity is the same, but the velocity field vanishes at a different rate depending upon the values of the power-law exponents q and n. The boundary layer thickness in (40) may be written as

$$\delta = \epsilon^{2-\alpha+\frac{(q-n)(1-\alpha)}{n+q}},$$

illustrating that it is thicker if $q < n$ and thinner if $q > n$ than that for UCM ($q = n = 1$). In fact, the boundary layer thickness is the same as UCM in the parameter regime $q = n$.

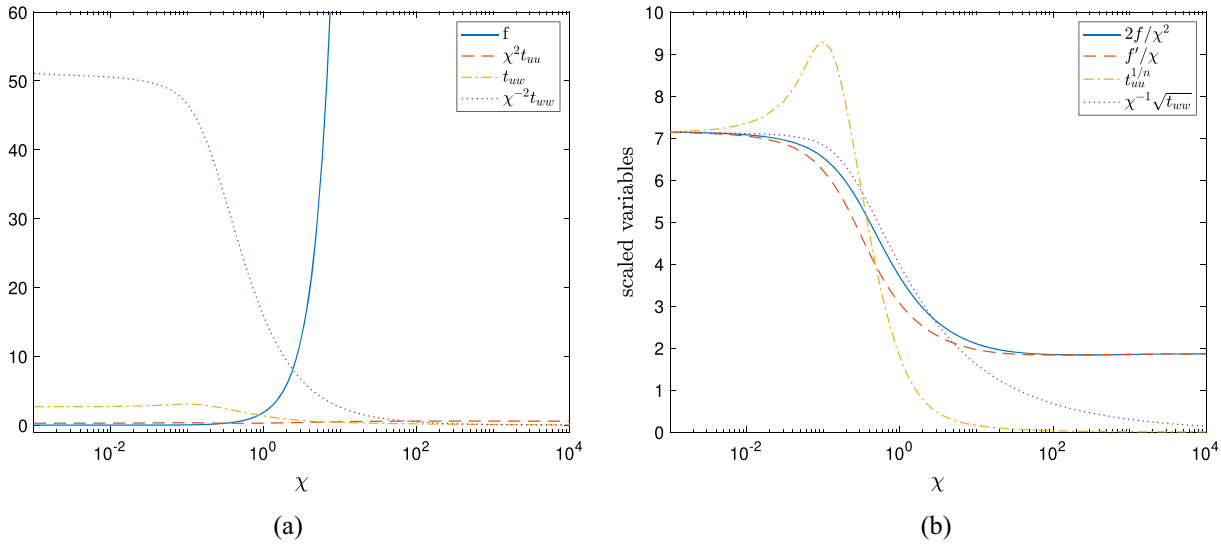

FIG. 4. The solution to the BVP (**a**) and functions that estimate the parameter f_{2d} (**b**) in the case of $n = 0.5$, $f_{2u} = -1$, $p_{0u} = 1$, $\alpha = 2/3$ on the interval $[10^{-3}, 10^4]$. Numerically, we find to four decimal places that at $\chi_0 = 10^{-3}$, $2f/\chi^2 = 7.1478$, $f'/\chi = 7.1414$, $t_{uw}^{1/n} = 7.1478$, $\sqrt{t_{ww}}/\chi = 7.1478$

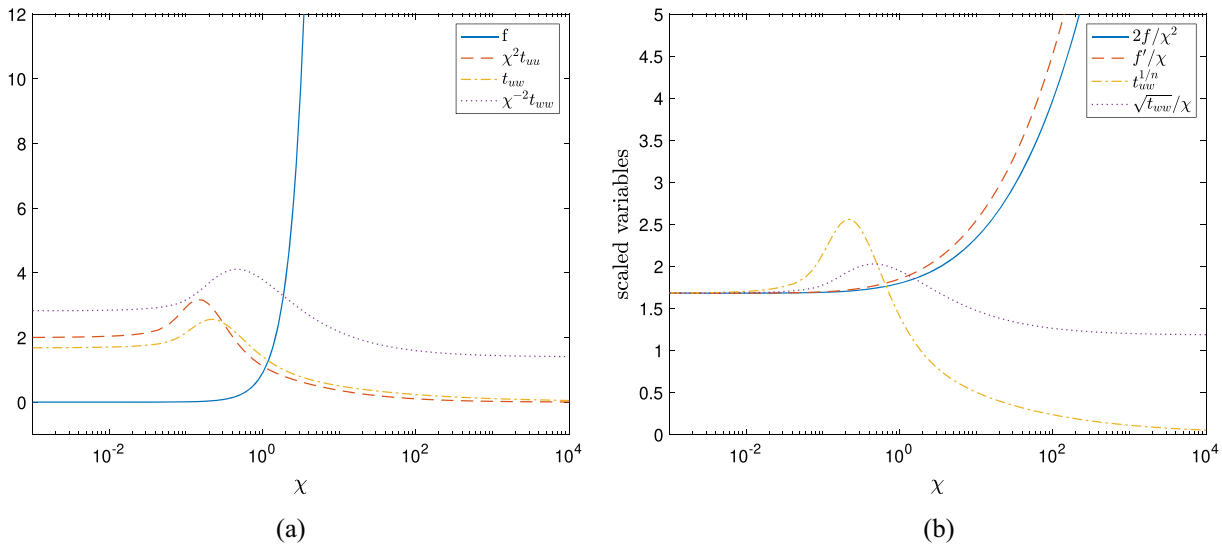

FIG. 5. The solution to the BVP (**a**) and functions that estimate the parameter f_{2d} (**b**) for the UCM model ($n = 1$), with $f_{2u} = -1$, $p_{0u} = 1$, $\alpha = 2/3$ on the interval $[10^{-3}, 10^4]$. Numerically, we find to four decimal places that at $\chi_0 = 10^{-3}$, $2f/\chi^2 = 1.6817$, $f'/\chi = 1.6812$, $t_{uw}^{1/n} = 1.6817$, $\sqrt{t_{ww}}/\chi = 1.6817$

Conditions on the power-law exponents for the validity of this solution are given in (30) and (31). Figure 7 illustrates the inequalities and the parameter region of interest. In summary, for shear thinning fluids $0 < n < 1$ we require $1 - n < q$. For shear thickening fluids $n > 1$ we require $q > \max(n - 2, 0)$. Outside of these regions, either the velocity field can develop a singularity at the corner or the upper convected

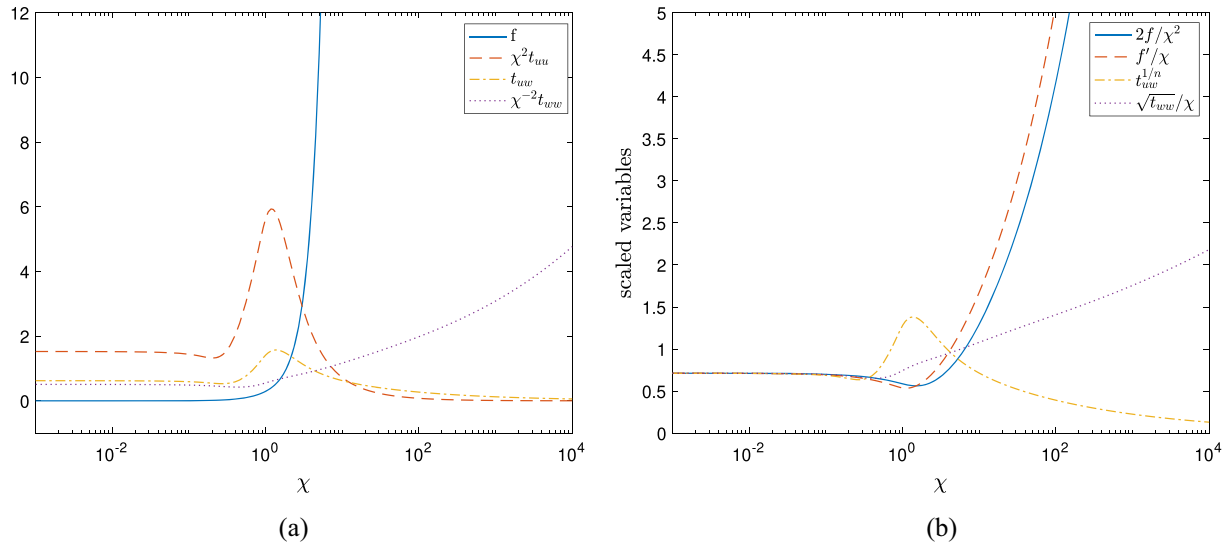

FIG. 6. The solution to the BVP (**a**) and functions that estimate the parameter f_{2d} (**b**) in the case of $n = 1.4$, $f_{2u} = -1$, $p_{0u} = 1$, $\alpha = 2/3$ on the interval $[10^{-3}, 10^4]$. Numerically, we find to four decimal places that at $\chi_0 = 10^{-3}$, $2f/\chi^2 = 0.7126$, $f'/\chi = 0.7125$, $t_{ww}^{1/n} = 0.7126$, $\sqrt{t_{ww}}/\chi = 0.7126$

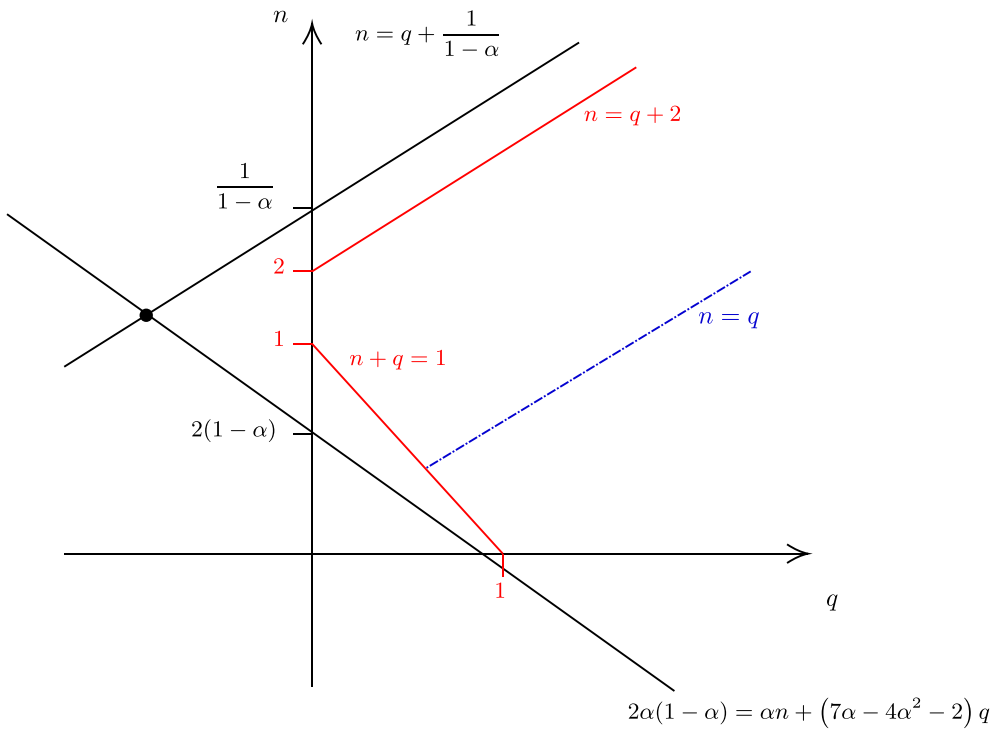

FIG. 7. A schematic illustrating the region of allowed values of n and q in terms of the corner parameter α. The lines $n + q = 1$ and $n = q + 2$ correspond to the case when the re-entrant corner angle is 2π ($\alpha = 1/2$). The "Bird equality" case $n = q$ is also found along the dot-dashed line

stress derivative no longer dominates the rate-of-strain terms in the constitutive equation. We note that in the "Bird equality" case $q = n$, we require $q = n > 1/2$ for validity of the solution, which we can extend to $q = n = 1/2$ if we exclude the full corner angle case $\alpha = 1/2$. In the introduction, we recorded some experimentally fitted values of n and q. We observe that some fall outside our required validity range, particularly when q is small. In these cases, use of the WM model in this form is questionable.

Acknowledgements

Christian Jones is supported by a scholarship from the EPSRC Centre for Doctoral Training in Statistical Applied Mathematics at Bath (SAMBa), under the Project EP/S022945/1. Jonathan Evans acknowledges support from FAPESP-SPRINT grant no. 2018/22242-0 and would like to thank the University of Bath for sabbatical leave during 2023-2024.

Author contributions JE conceptualised the project. CJ and JE performed the mathematical analysis and CJ the numerical computations. Both JE and CJ contributed to the drafting, review and editing of the manuscript, and both authors have read and agreed to the final version of the manuscript.

Data availability statement No datasets were generated or analysed during the current study.

Declarations
Conflict of interest The authors declare no Conflict of interest.

Appendix A. Cartesian formulation

As we intend to reconcile some of our results with those in [4], it is worth mentioning the formulation of Eqs. (11) and (12) in Cartesian coordinates. For our problem, we make the choice of Cartesian axes with the x-axis along the upstream wall ($\theta = 0$), and the y-axis along the ray $\theta = \pi/2$. Writing the velocity as $\mathbf{u} = (u, v)^T$, we have that the momentum equations (11) are

$$(\mathbf{u} \cdot \nabla)\, u = -\frac{\partial p}{\partial x} + \frac{\partial T_{11}}{\partial x} + \frac{\partial T_{12}}{\partial y}, \tag{67}$$

$$(\mathbf{u} \cdot \nabla)\, v = -\frac{\partial p}{\partial y} + \frac{\partial T_{12}}{\partial x} + \frac{\partial T_{22}}{\partial y}, \tag{68}$$

alongside the constitutive equations (12), given by

$$T_{11} + \dot{\gamma}^{q-1}\left(u\frac{\partial T_{11}}{\partial x} + v\frac{\partial T_{11}}{\partial y} - 2\frac{\partial u}{\partial y}T_{12} - 2\frac{\partial u}{\partial x}T_{11}\right) = 2\dot{\gamma}^{n-1}\frac{\partial u}{\partial x}, \tag{69}$$

$$T_{12} + \dot{\gamma}^{q-1}\left(u\frac{\partial T_{12}}{\partial x} + v\frac{\partial T_{12}}{\partial y} - \frac{\partial v}{\partial x}T_{11} - \frac{\partial u}{\partial y}T_{22}\right) = \dot{\gamma}^{n-1}\left(\frac{\partial u}{\partial y} + \frac{\partial v}{\partial x}\right), \tag{70}$$

$$T_{22} + \dot{\gamma}^{q-1}\left(u\frac{\partial T_{22}}{\partial x} + v\frac{\partial T_{22}}{\partial y} - 2\frac{\partial v}{\partial x}T_{12} - 2\frac{\partial v}{\partial y}T_{22}\right) = 2\dot{\gamma}^{n-1}\frac{\partial v}{\partial y}. \tag{71}$$

The quantities T_{ij} refer to the Cartesian components of the extra stress tensor, with the indices 1 and 2 identifying the x and y axes, respectively.
In the boundary layers, we introduce the scaled variables

$$T_{11} = \epsilon^{2(\alpha-1)}\bar{T}_{11}, \quad T_{12} = \epsilon^{\frac{2n(\alpha-1)}{n+q}}\bar{T}_{12}, \quad T_{22} = \epsilon^{\frac{2(n-q)(\alpha-1)}{n+q}}\bar{T}_{22}, \tag{72}$$

alongside those in (34), to obtain the Cartesian form of the boundary layer equations as found in [4]:

$$0 = -\frac{\partial \bar{p}}{\partial X} + \frac{\partial \bar{T}_{11}}{\partial X} + \frac{\partial \bar{T}_{12}}{\partial Y}, \tag{73}$$

$$0 = \frac{\partial \bar{p}}{\partial Y}, \tag{74}$$

with corresponding WM equations

$$\bar{T}_{11} + \left|\frac{\partial \bar{u}}{\partial Y}\right|^{q-1}\left[\left(\bar{\mathbf{u}}\cdot\bar{\nabla}\right)\bar{T}_{11} - 2\frac{\partial \bar{u}}{\partial X}\bar{T}_{11} - 2\frac{\partial \bar{u}}{\partial Y}\bar{T}_{22}\right] = 0, \tag{75}$$

$$\bar{T}_{12} + \left|\frac{\partial \bar{u}}{\partial Y}\right|^{q-1}\left[\left(\bar{\mathbf{u}}\cdot\bar{\nabla}\right)\bar{T}_{12} - \frac{\partial \bar{v}}{\partial X}\bar{T}_{11} - \frac{\partial \bar{u}}{\partial Y}\bar{T}_{22}\right] = \left|\frac{\partial \bar{u}}{\partial Y}\right|^{n-1}\frac{\partial \bar{u}}{\partial Y}, \tag{76}$$

$$\bar{T}_{22} + \left|\frac{\partial \bar{u}}{\partial Y}\right|^{q-1}\left[\left(\bar{\mathbf{u}}\cdot\bar{\nabla}\right)\bar{T}_{22} - 2\frac{\partial \bar{v}}{\partial X}\bar{T}_{12} - 2\frac{\partial \bar{v}}{\partial Y}\bar{T}_{22}\right] = 2\left|\frac{\partial \bar{u}}{\partial Y}\right|^{n-1}\frac{\partial \bar{v}}{\partial Y}. \tag{77}$$

Applying these boundary layer scalings to the conformation tensor representation in (16), we find that at leading order in ϵ, the Cartesian and natural stress components are related by

$$\bar{T}_{11} = \bar{T}_{uu}\bar{u}^2 \tag{78}$$

$$\bar{T}_{12} = \bar{T}_{uu}\bar{u}\bar{v} + \bar{T}_{uw}, \tag{79}$$

$$\bar{T}_{22} = -\left|\frac{\partial \bar{u}}{\partial Y}\right|^{n-q} + \bar{T}_{uu}\bar{v}^2 + \frac{2\bar{T}_{uw}\bar{v}}{\bar{u}} + \frac{\bar{T}_{ww}}{\bar{u}^2}. \tag{80}$$

Finally, it can be shown that the system of Eqs. (73)–(77) possesses a similarity solution in the variable

$$\chi = X^{-a}Y,$$

with

$$\bar{\psi} = X^b f(\chi), \quad \bar{p} = X^{2\alpha-2}p_0, \quad \bar{T}_{11} = X^{2(\alpha-1)}t_{11}(\chi),$$
$$\bar{T}_{12} = X^{2(\alpha-1)m_{12}}t_{12}(\chi), \quad \bar{T}_{22} = X^{2(\alpha-1)(m_{12}-m_{22})}t_{22}(\chi).$$

Here, a and b are defined as in (46), and we have additionally introduced

$$m_{12} = \frac{n}{n+q}, \qquad m_{22} = \frac{q}{n+q}.$$

In this case, the system of PDEs reduces to the four ODEs:

$$0 = 2(1-\alpha)p_0 - a\chi t_{11}' + t_{12}' + 2(\alpha-1)t_{11},$$
$$|f''|^{1-q}t_{11} = bft_{11}' + \left[2(1-\alpha+b-a)f' - 2a\chi f''\right]t_{11} + 2f''t_{12},$$
$$|f''|^{1-q}t_{12} = bft_{12}' + 2(1-\alpha)m_{12}f't_{12} + \left[b(1-b)f + a(2b-a-1)\chi f' - a^2\chi^2 f''\right]t_{11}$$
$$+ \left(t_{22} + |f''|^{n-q}\right)f'',$$
$$|f''|^{1-q}t_{22} = bft_{22}' - \left[2b(b-1)f + 2a(a+1-2b)\chi f' + 2a^2\chi^2 f''\right]t_{12}$$
$$+ 2\left[a\chi f'' + (a-b-(\alpha-1)(m_{12}-m_{22}))f'\right]t_{22} + 2\left(a\chi f'' + (a-b)f'\right)|f''|^{n-q},$$

subject to the boundary conditions

$$\text{at } \chi = 0: \qquad f = f' = 0,$$
$$\text{as } \chi \to \infty: \qquad f \sim C_0 \chi^m, \quad t_{11} \sim 2p_0, \quad t_{12} \sim 2(1-\alpha)p_0\chi, \quad t_{22} \sim 2(1-\alpha)^2 p_0 \chi^2.$$

We note that the far-field outer matching behaviour does not contain the constants d_2, d_3 and hence the upstream solution in these variables can only supply the leading order behaviour of the stresses in the outer region. Further terms in the outer expansion are required in order to obtain the necessary information to supply to the downstream boundary layer.

References

[1] White, J.L., Metzner, A.B.: Development of constitutive equations for polymeric melts and solutions. J. Appl. Polym. Sci. **7**, 1867–1889 (1963). https://doi.org/10.1002/app.1963.070070524

[2] Bird, R.B., Armstrong, R.C., Hassager, O.: Dynamics of Polymeric Liquids, vol. 1, 2nd ed. Fluid mechanics, New York (1987)

[3] Sousa, P.C., et al.: Purely elastic flow instabilities in microscale cross-slot devices. Soft Matter **11**, 8856–8862 (2015). https://doi.org/10.1039/C5SM01298H

[4] Chaffin, S., et al.: Re-entrant corner for a White–Metzner fluid. Fluids (2021). https://doi.org/10.3390/fluids6070241

[5] Liao, T.Y., Hu, H.H., Joseph, D.D.: White–Metzner models for rod climbing in A1. J. Non-Newton. Fluid Mech. **51**, 111–124 (1994). https://doi.org/10.1016/0377-0257(94)85007-0

[6] Valette, R., et al.: Investigation of the interfacial instabilities in the coextrusion flow of PE and PS. Int. Polym. Proc. **18**, 171–178 (2003). https://doi.org/10.3139/217.1731

[7] Khan, S.A., Larson, R.G.: Comparison of simple constitutive equations for polymer melts in shear and biaxial and uniaxial extensions. J. Rheol. **31**, 207–234 (1987). https://doi.org/10.1122/1.549922

[8] Dupret, F., Marchal, J.M.: Loss of evolution in the flow of viscoelastic fluids. J. Non-Newton. Fluid Mech. **20**, 143–171 (1986). https://doi.org/10.1016/0377-0257(86)80019-2

[9] Verdier, C., Joseph, D.D.: Change of type and loss of evolution of the White–Metzner model. J. Non-Newton. Fluid Mech. **31**, 325–343 (1989). https://doi.org/10.1016/0377-0257(89)85004-9

[10] Maders, H., et al.: Steady flow of a White–Metzner fluid in a 2-D abrupt contraction: computation and experiments. J. Non-Newton. Fluid Mech. **45**, 63–80 (1992). https://doi.org/10.1016/0377-0257(92)80061-2

[11] Raghay, S., Hakim, A.: Numerical simulation of White-Metzner fluid in a 4:1 contraction. Int. J. Numer. Methods Fluids **35**, 559–573 (2001). https://doi.org/10.1002/1097-0363(20010315)35:5⟨559::AID-FLD102⟩3.0.CO;2-P

[12] Dhanasekharan, M., Huang, H., Kokini, J.L.: Comparison of observed rheological properties of hard wheat flour dough with predictions of the Giesekus–Leonov, White–Metzner and Phan–Thien Tanner models. J. Texture Stud. **30**, 603–623 (1999). https://doi.org/10.1111/j.1745-4603.1999.tb00233.x

[13] Metzner, A.B., Whitlock, M.: Flow behavior of concentrated (dilatant) suspensions. Trans. Soc. Rheol. **2**, 239–254 (1958). https://doi.org/10.1122/1.548831

[14] Strivens, T.A.: The shear thickening effect in concentrated dispersion systems. J. Colloid Interface Sci. **57**, 476–487 (1976). https://doi.org/10.1016/0021-9797(76)90226-5

[15] Boersma, W.H., Laven, J., Stein, H.N.: Viscoelastic properties of concentrated shear-thickening dispersions. J. Colloid Interface Sci. **149**, 10–22 (1992). https://doi.org/10.1016/0021-9797(92)90385-Y

[16] Lipscomb, G.G., Keunings, R., Denn, M.M.: Implications of boundary singularities in complex geometries. J. Non-Newton. Fluid Mech. **24**, 85–96 (1987). https://doi.org/10.1016/0377-0257(87)85005-X

[17] Singh, P., Leal, L.G.: Finite element simulation of flow around a $3\pi/2$ corner using the FENE dumbbell model. J. Non-Newton. Fluid Mech. **58**, 279–313 (1995). https://doi.org/10.1016/0377-0257(95)01346-W

[18] Evans, J.D.: Re-entrant corner flows of the upper convected Maxwell fluid. Proc. R. Soc. A. **461**, 117–142 (2005). https://doi.org/10.1098/rspa.2004.1335

[19] Evans, J.D.: Re-entrant corner flows of UCM fluids: the Cartesian stress basis. J. Non-Newton. Fluid Mech. **150**, 116–138 (2008). https://doi.org/10.1016/j.jnnfm.2007.10.018

[20] Evans, J.D.: Re-entrant corner flows of UCM fluids: the natural stress basis. J. Non-Newton. Fluid Mech. **150**, 139–153 (2008). https://doi.org/10.1016/j.jnnfm.2007.10.019

[21] Trebotich, D., Colella, P., Miller, G.H.: A stable and convergent scheme for viscoelastic flow in contraction channels. J. Comput. Phys. **205**, 315–342 (2005). https://doi.org/10.1016/j.jcp.2004.11.007

[22] Renardy, M.: How to integrate the upper convected Maxwell (UCM) stresses near a singularity (and maybe elsewhere, too). J. Non-Newton. Fluid Mech. **52**, 91–95 (1994). https://doi.org/10.1016/0377-0257(94)85060-7

[23] Renardy, M.: The high Weissenberg number limit of the UCM model and the Euler equations. J. Non-Newton. Fluid Mech. **69**, 293–301 (1997). https://doi.org/10.1016/S0377-0257(96)01544-3
[24] Hinch, E.J.: The flow of an Oldroyd fluid around a sharp corner. J. Non-Newton. Fluid Mech. **50**, 161–171 (1993). https://doi.org/10.1016/0377-0257(93)80029-B
[25] Rallison, J.M., Hinch, E.J.: The flow of an Oldroyd fluid past a reentrant corner: the downstream boundary layer. J. Non-Newton. Fluid Mech. **116**, 141–162 (2004). https://doi.org/10.1016/j.jnnfm.2003.10.001
[26] Renardy, M.: A matched solution for corner flow of the upper convected Maxwell fluid. J. Non-Newton. Fluid Mech. 58, 83-89 (1995). https://doi.org/10.1016/0377-0257(94)01339-J

Jonathan D. Evans and Christian A. Jones
Department of Mathematical Sciences
University of Bath
Bath BA2 7AY
UK
e-mail: caj50@bath.ac.uk

Jonathan D. Evans
e-mail: masjde@bath.ac.uk

(Received: February 12, 2024; revised: February 12, 2024; accepted: February 26, 2024)